Ecological Indicators 136 (2022) 108630

Contents lists available at ScienceDirect

Ecological Indicators

journal homepage: www.elsevier.com/locate/ecolind

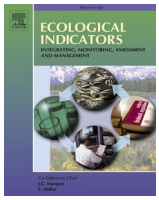

Original Articles

Responding time scales of vegetation production to extreme droughts over China

Ying Deng [a,*], Donghai Wu [b], Xuhui Wang [c], Zongqiang Xie [a]

[a] State Key Laboratory of Vegetation and Environmental Change, Institute of Botany, Chinese Academy of Sciences, No. 20 Nanxincun, Xiangshan, Beijing 100093, China
[b] Department of Ecology and Evolutionary Biology, Cornell University, Ithaca NY 14850, USA
[c] Sino-French Institute for Earth System Science, College of Urban and Environmental Sciences, Peking University, Beijing 100871, China

ARTICLE INFO

Keywords:
Standardized Precipitation Evapotranspiration Index (SPEI)
Gross Primary Productivity (GPP)
Time scale
Extreme droughts
Linear correlation

ABSTRACT

Extreme drought events have caused extensive and severe impacts on terrestrial ecosystem in last decades in China. Given droughts may be more intense and frequent under future climate change, accurate assessment of the drought impact on vegetation primary production can provide reliably scientific supports for the carbon sink potential. Numerous existing studies have used Standardized Precipitation Evapotranspiration Index (SPEI) to discover the drought-production relationships, however, most of them just considered the strongest correlation between production and different time scales (i.e. correlation-based method), which may underestimate the production loss because of the asymmetric responses under dry and wet conditions. In this work, we proposed a new method which assumed that the dominant time scale should correspond to the lowest primary production during each drought year (extreme-based method). Based on six independent Gross Primary Productivity (GPP) products and SPEI dataset, it showed that the extreme-based method was more reasonable and robust (with a larger inter-consistency of 0.50 than that of 0.05 for correlation-based method) to determine at which time scale GPP predominantly responded to extreme droughts. And the GPP loss can be underestimated by 45 ± 26% (mean ± s.d.) if the time scale was randomly selected. Furthermore, spatial analysis suggested that vegetation type, water balance and soil textures mainly affected the spatial heterogeneity of the dominant time scales. In detail, forests, humid biomes, and vegetation planted in loam tended to be more sensitive to longer-term droughts. This study highlighted that optimal time-scale selection using extreme-based assumption can give more accurate estimation of the drought impacts on vegetation primary production.

1. Introduction

During the recent decades, many regions have experienced extreme droughts around the globe, such as the 2005 and 2010 drought over Amazonia (Doughty et al., 2015; van der Laan-Luijkx et al., 2015), the 2012 summer drought in the US (Wolf et al., 2016), and the 2009/10 drought and heatwave in southwest China (Li et al., 2019; Zhao et al., 2015). It is observed those extreme droughts caused severe impacts on vegetation growth and carbon cycle (Wu et al., 2021; Zhao and Running, 2010), and it will be even aggravated given the changing climate (Xu et al., 2019). That is, studying how carbon cycle particularly the photosynthesis process responds to extreme droughts is crucial.

Nevertheless, there has not received a consistent definition of drought since it is difficult to describe droughts in time and space (Mishra and Singh, 2010). More than 50 drought indicators (World Meteorological Organization and Global Water Partnership, 2016) and water balancing frameworks (Maurya et al., 2020) are developed to address this practical issue. And standardized metrics are highly recommended and assumed to better indicate droughts and enable comparisons across locations and biomes, since droughts imply a deficit in water availability that differ from normal (Slette et al., 2019; Slette et al., 2020). Besides, drought conditions may be different when being calculated based on different periods of climate context. In general, short-term water shortage connects with vegetation growth and is namely meteorological droughts, while longer-term water imbalance will lead to streamflow decrease, soil moisture deficit, and even failures on water resource systems (Mishra and Singh, 2010; Wu et al., 2018).

The Standardized Precipitation Evapotranspiration Index (SPEI), on the one hand, is a standardized metric considering both precipitation and evapotranspiration (that is, water balance); on the other hand, can

* Corresponding author.
E-mail address: yingdeng@ibcas.ac.cn (Y. Deng).

https://doi.org/10.1016/j.ecolind.2022.108630
Received 9 November 2021; Received in revised form 19 January 2022; Accepted 28 January 2022
Available online 3 February 2022

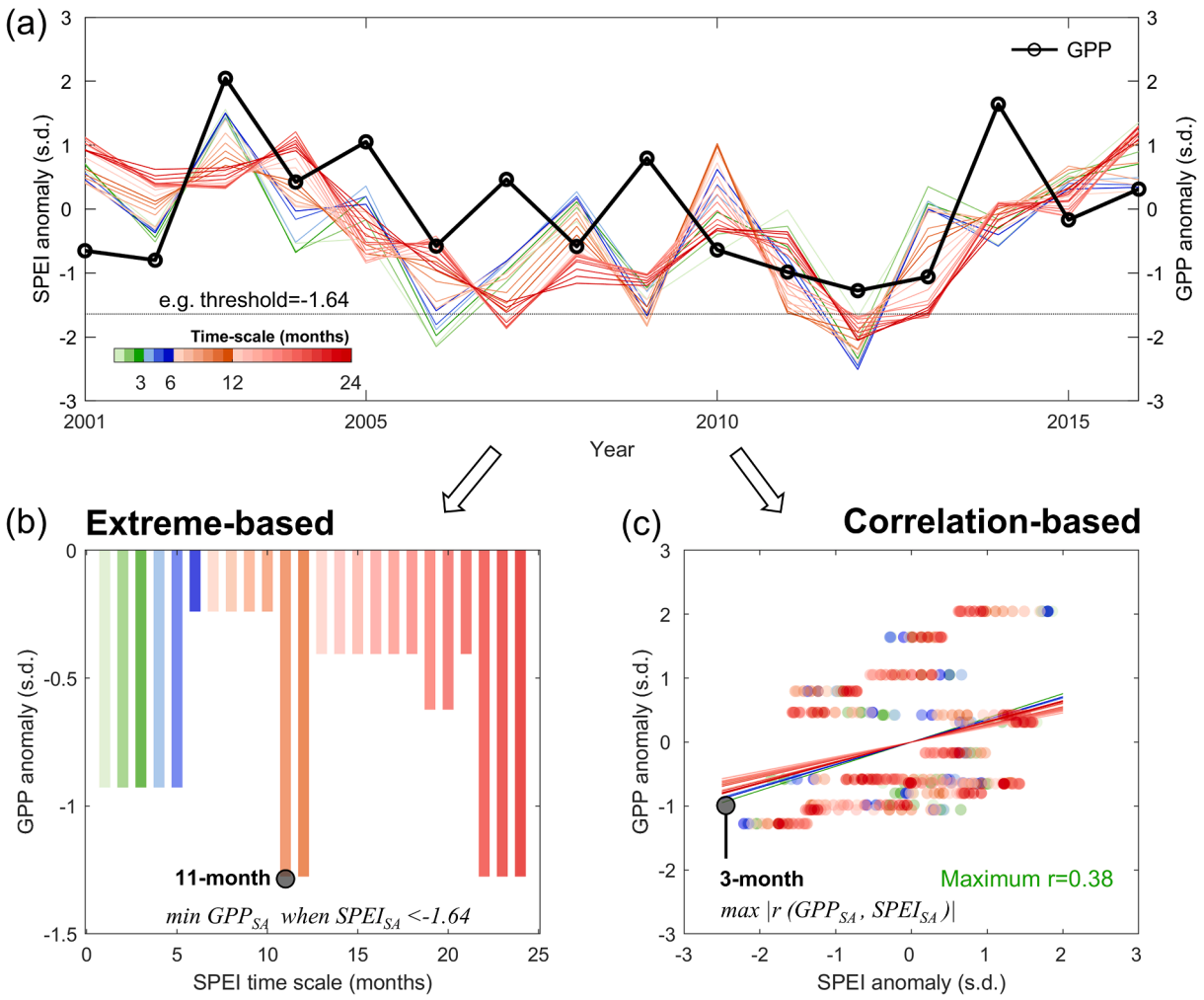

Fig. 1. An example of deriving dominant time scales from extreme and correlation perspectives. Standardized anomaly of annual mean SPEI ($SPEI_{SA}$) at time scales of 1–24 month and mean GPP (GPP_{SA}) at one pixel are shown in Fig. 1a. As in this example, dominant time scale derived from extreme-based method (b) is 11-month since mean GPP_{SA} during extreme drought years (when $SPEI_{SA}$ was less than −1.64) firstly reaches the minimum. And the scale derived from correlation-based method (c) is 3-month since the Spearman correlation coefficient between annual GPP_{SA} and $SPEI_{SA}$ reaches the maximum.

indicate droughts of different time scales (Vicente-Serrano et al., 2010a): thus was widely used particularly for large-scale and long-term drought researches (Anderegg et al., 2020; Schwalm et al., 2017). Numerous studies employed a Pearson's correlation analysis between SPEI at different time scales and vegetation-related indices, and found vegetation and carbon fluxes may respond to droughts at different time scales (Vicente-Serrano et al., 2013). Specifically, for arid and humid areas, vegetation greenness and productivity responded to short-term droughts although through different physiological mechanisms, while semi-arid and semi-humid biomes tended to respond to longer-term droughts (Vicente-Serrano et al., 2013). Further, the forest was more sensitive to long-term droughts rather than grassland and cropland due to the rooting system and soil texture (Jiang et al., 2020).

However, it remains uncertain whether the largest linear correlation coefficient is reasonable for selecting an optimal response time scale. First, responses of vegetation productivity to precipitation tend to be asymmetric, which might show a smaller increase of productivity in wet years than the decline in dry years, or in the opposite way (Knapp et al., 2017). A recent study of America using multiple Gross Primary Productivity (GPP) data sources has revealed a consistent spatial pattern of the asymmetry, and the Great Plains indicated a negative asymmetry (a greater decline in dry years) and the Southwest positive (Al-Yaari et al., 2020). Besides, correlations between SPEI and tree ring index showed a tipping point and turned to be much weaker under non-extreme dry conditions (Huang et al., 2015). In this way, linear fit might not well portray the true response of vegetation growth in extreme wet or dry conditions. Second, the correlation coefficients on whole time series are highly affected by extreme values and may be not valid when variables are not normally distributed (Mukaka, 2012). Furthermore, Pearson's correlation coefficients may reflect relationships between general vegetation growth and water content condition, but fail to concentrate on samples from extreme situations, the range of which should be truly concerned for studying droughts. Thus, as one of the most severe climate extremes (Reichstein et al., 2013; Zscheischler et al., 2014), droughts may lead to abrupt tree mortality and sudden system failure (Allen et al., 2010), and linear correlation approach may not be appropriate for studying vegetation response to droughts.

Drought affected areas have been doubled in China during the last three decades (Xu et al., 2012), and will continue to increasing under the background of climate warming (Su et al., 2018). There areas were also accompanied by a decreasing greenness and a decline of carbon uptake (Deng et al., 2021). For example, the 2013 drought and heat wave caused a reduction of 101.54 Tg C in carbon sequestration in southern China (Yuan et al., 2016). In this sense, we took China as the study area and re-considered the issue of how vegetation photosynthesis responds to droughts but under extreme situations: (1) Which time scale of extreme droughts lead to most ecosystem Gross Primary Productivity (GPP) loss? (2) Is the dominant scale different from that derived by the

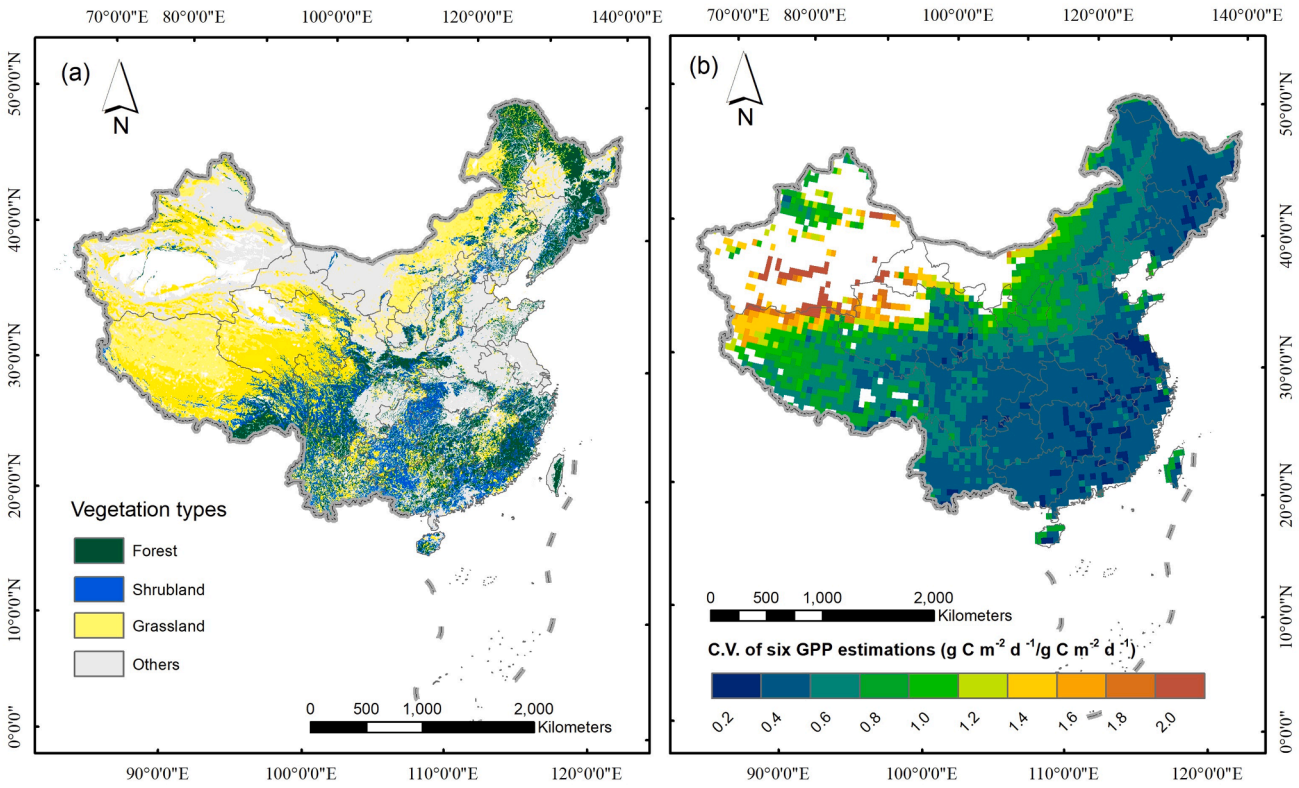

Fig. 2. Study area (a) and uncertainties of GPP from different products (b). Land cover data was adapted from the 1:1,000,000 digitalized vegetation map of China (Editorial Board of Vegetation Map of China, 2007). Forest, shrubland and grassland areas were analyzed. Information of Six GPP estimations or simulations is shown in Table 1, and uncertainty was measured by the Coefficient of Variation (C.V.) among the products.

Table 1
Data sources used in this study.

Indicators	Products		Spatial resolution	Temporal resolution	References
SPEI	SPEI v2.5		0.5°	monthly	Vicente-Serrano et al., 2010b
GPP	MODIS GPP C5.5		500 m	8-day	Chen et al., 2021; Zhao et al., 2005
	P-model		0.5°	daily	Stocker et al., 2018; Stocker et al., 2019
	VODCA2GPP		0.25°	8-day	Wild et al., 2021
	MTE GPP China		0.1°	monthly	Li et al., 2019; Yao et al., 2018
	FLUXCOM upscaling		1°	monthly	He et al., 2021; Tramontana et al., 2016
	TRENDYv8		0.5° ~ 2.8125°	monthly	Le Quéré et al., 2018; Piao et al., 2020
Others	CSIF		0.05°	4-day	Chen et al., 2021; Zhang et al., 2018
	NIRv		0.1°	monthly	Badgley et al., 2017; Huang et al., 2019
Fire emissions	GFED v4.1		0.25°	monthly	Randerson et al., 2017
Environmental factors	Precipitation	CRU TS 4.03	0.5° × 0.5°	monthly	Harris et al., 2020
	Potential evapotranspiration				
	Soil texture		0.0083° × 0.0083°	none	Resources and Environmental Sciences, Chinese Academy of Sciences (RESDC)

linear correlation method? (3) Whether drought impacts will be under (over) estimated if time scale and thresholds are not carefully selected? By addressing the above questions, we combined six state-of-the-art GPP products derived from remote sensing observations, FLUXNET upscale approach and process-based model simulations. Given that GPP can hardly be measured at large ecosystem scales, two additional indices Contiguous Solar-induced Fluorescence (CSIF) and Near-Infrared Reflectance of vegetation (NIRv), which are suggested to strongly correlated with GPP signals, were provided as well.

2. Materials and methods

2.1. Methodology

In this study, we tended to compare the dominant drought scale derived from the extreme and correlation perspectives (following most previous studies (Vicente-Serrano et al., 2013)). From the extreme perspective, drought is described as an extremely low water availability from the normal level, that is, standardized anomaly (SA) of SPEI is below one threshold. Then the threshold and the time scale of SPEI are concerned when defining an extreme drought year. Thus, we examined the GPP response (SA of GPP) during extreme drought years defined by different combinations of SPEI time scales and thresholds, and the dominant time scale is the shortest time scale of SPEI under which the

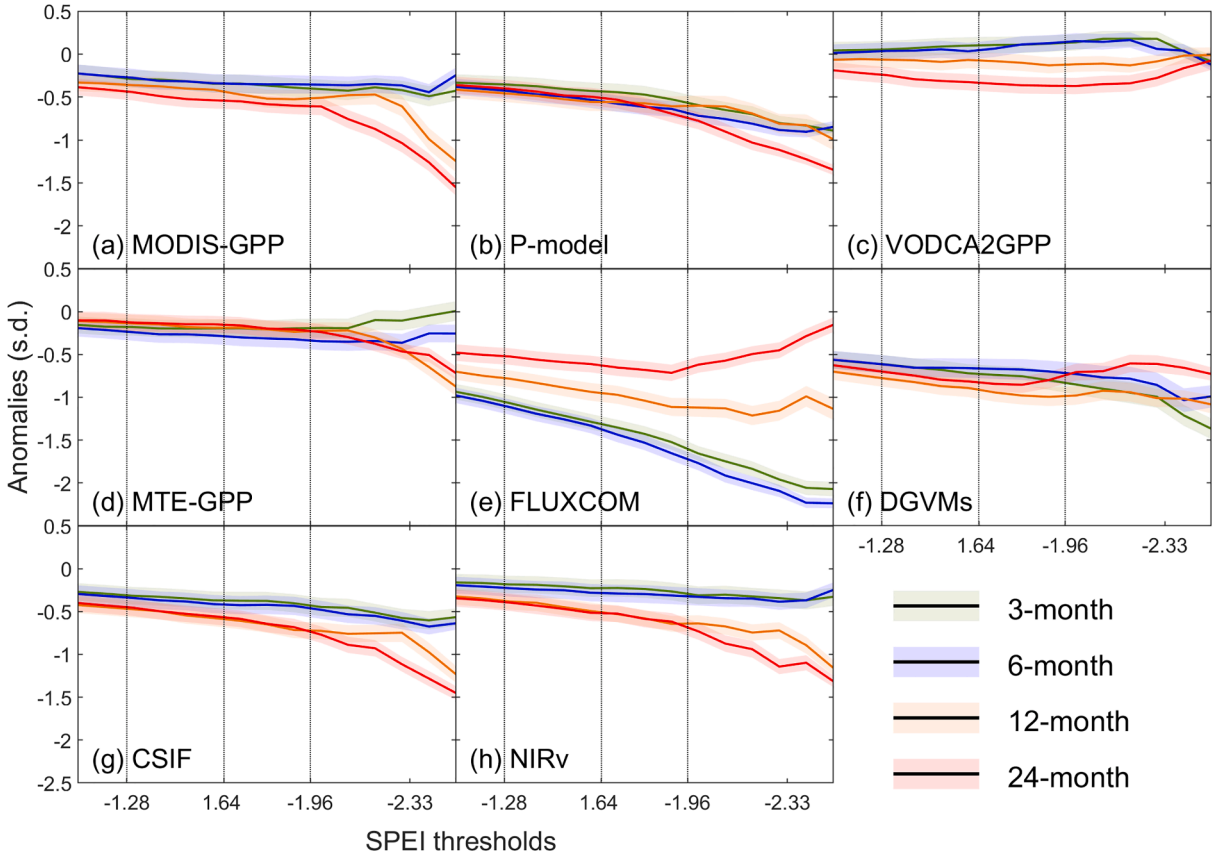

Fig. 3. Mean GS-GPP anomalies (s.d.) during extreme drought years defined by different thresholds. Extreme drought years were defined using 3, 6, 12, and 24-month time scale of SPEI, and thresholds from −1 – −2.5 with a bin length of 0.1. Shaded areas show the range of ± 10% standard deviation.

most negative GPP response was observed (Eq.(1)).

$$SA_{s,t}(\mathrm{GPP}) = \min\left[SA_{s,1}(\mathrm{GPP}), SA_{s,2}(\mathrm{GPP}), \cdots, SA_{s,24}(\mathrm{GPP})\right] \quad (1)$$

where $SA_{s,t}(\mathrm{GPP})$ is the minimum value of standardized anomaly of GPP during drought years defined by SPEI from 1-month scale to 24-month scale under one particular threshold, and the t is the dominant drought time scale. If more than one time -scale of SPEI share the same GPP response, the shortest time scale should be the dominant time scale.

From the correlation perspective, drought is described as a general dry condition over the period, that is, the dominant drought time scale is identified by the linear correlation method just as in previous studies (Gouveia et al., 2017; Jiang et al., 2020; Li et al., 2018). And the dominant drought time scale is the time scale under which the strongest Spearman's correlation between annual SPEI and GPP was observed (Eq. (2)).

$$|\mathrm{R}(\mathrm{GPP}, SPEI_t)| = \max[|\mathrm{R}(\mathrm{GPP}, SPEI_1)|, |\mathrm{R}(\mathrm{GPP}, SPEI_2)|, \cdots, |\mathrm{R}(\mathrm{GPP}, SPEI_{24})|] \quad (2)$$

where $|\mathrm{R}(\mathrm{GPP}, SPEI_t)|$ is the maximum value of the absolute correlation coefficient between GPP and SPEI from 1-month scale to 24-month scale, and the t is the dominant drought time scale.

To better illustrate the differences, Fig. 1 shows an example of how dominant SPEI time scale was derived from these two perspectives. For a given pixel, annual time series of SPEI at 1–24 month scales and GPP were in Fig. 1a: from the extreme perspective, extreme drought years were defined when SPEI was below one threshold. Here we chose −1.64 as the threshold since the probability of 5% is always regarded as an extreme event (IPCC, 2014), and the left-tail probability of a normal distribution is 5% when the z-score is below −1.64. Then mean GPP responses during drought years were calculated, and the dominant time scale was at which scale minimum GPP response was firstly reached (Fig. 1b, 11-month); from the correlation perspective, Spearman's correlation coefficients between SPEI and GPP (annual values from Fig. 1a) were calculated, and the dominant time scale was at which scale the strongest correlation was found (Fig. 1c, 3-month).

2.2. Study area

The study area China locates between 3°N ~ 54°N and 73°E ~ 136°E, with large climate gradients and rich vegetation cover. Fig. 2a shows the vegetation cover, and the data was derived and adapted from the 1:1,000,000 digitalized vegetation map of China (Editorial Board of Vegetation Map of China, 2007). The majority of forests and shrublands locate in the south and part of the northeast, croplands spread over continuous areas in North China Plain and Sichuan Basin, grasslands distributes widely in arid and semi-arid north and northeast China. In case of the unavoidable impacts of human management, croplands were removed for analysis. The various vegetation cover and complex topography constitute a challenge for precise GPP estimation or simulation. It is observed uncertainties among different GPP products could be large, the Coefficient of Variation (C.V.) is more than 1.5 g C m^{-2} d^{-1} in alpine vegetation (Fig. 2b). Generally, the uncertainty decreased from the northwest to the southeast, exhibiting a changing gradient.

2.3. Datasets

Detailed information of the data sources is shown in Table 1. The drought indicator SPEI (Vicente-Serrano et al., 2010a; Vicente-Serrano et al., 2010b) was used to identify extreme drought years, and temporal resolution of the data was monthly, and spatial resolution was 0.5° × 0.5°.

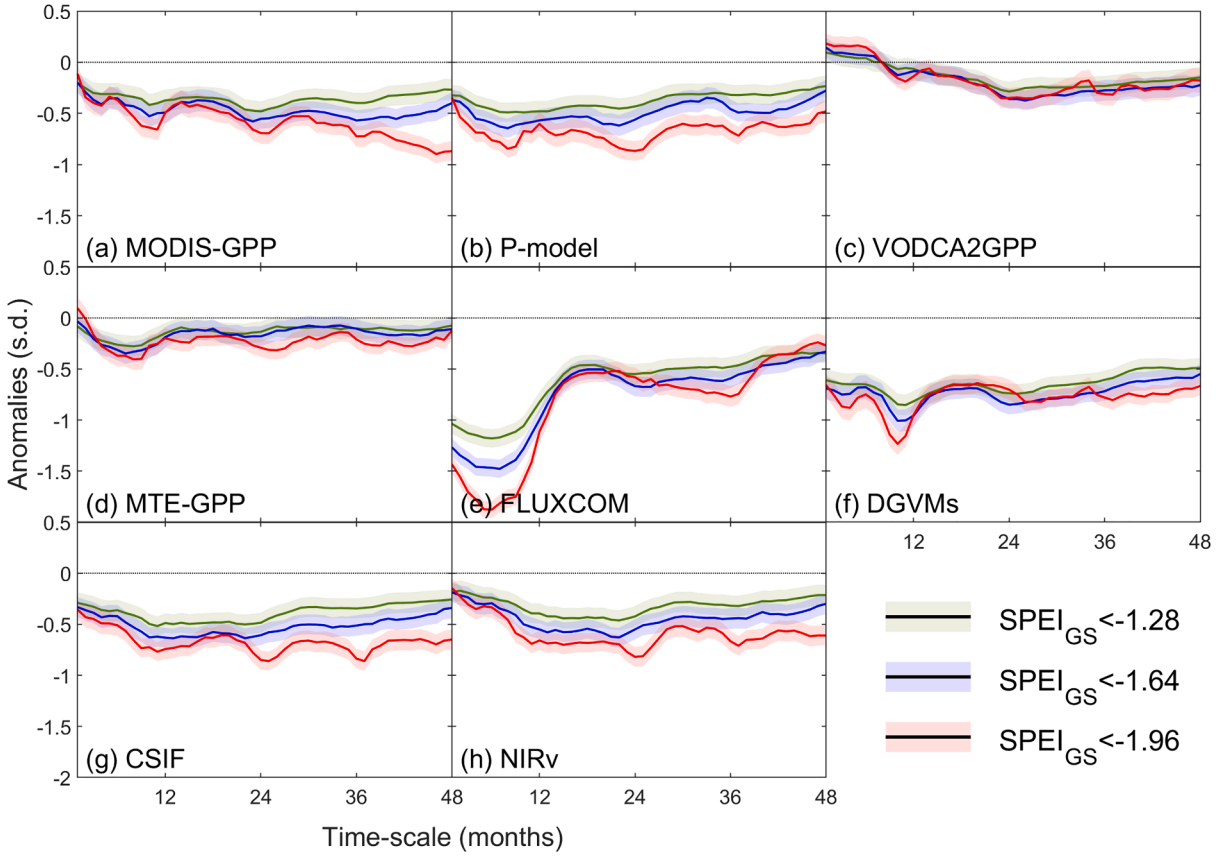

Fig. 4. Mean GS-GPP anomalies during extreme drought years defined by different time scales of SPEI. Extreme drought years were defined using thresholds of −1.28, −1.64, and −1.96, and time scales of SPEI from 1-month to 48-month. Shaded areas show the range of ± 10% standard deviation.

Large-scale ecosystem GPP can be acquired from at least three primary means (Zhang et al., 2016). Light Use Efficiency (LUE) and remote sensing observations based GPP: this method assumes that GPP is the function of canopy absorbed photosynthetically active radiation and LUE (Zhao et al., 2005). The former can be sensed by satellites sensors, and the latter can be expressed as a function of environmental stress (such as temperature and soil moisture). Flux sites observation upscaling approach: it constructs a relationship between flux tower observed GPP and other biotic or environmental factors, and upscales GPP by the relationship and the gridded data of those driving factors (Jung et al., 2020). The upscaling GPP can well present spatial heterogeneity, but may underestimate the inter-annual variations (Anav et al., 2015). Process-based model simulations: the models simulate ecological processes of carbon cycle based on assumptions of ecosystem structures and how they respond to climate change (Sitch et al., 2008). There may exist uncertainties among model-simulated GPP, since the models are simplified and have the limitation to reflect the complicated ecosystems particularly under intense human disturbances (Xie et al., 2020).

Here six state-of-the-art GPP products were used to provide a general picture of ecosystem primary productivity responses: 1) MODIS-GPP (Zhao et al., 2005) based on LUE and remote sensing observations; 2) P-model GPP (Stocker et al., 2019), based on LUE as well but considering effects of soil moisture while MODIS-GPP used Vapor Pressure Deficit (VPD) as a water stress; 3) VODCA2GPP (Wild et al., 2021), which was trained by microwave remote sensing observed Vegetation Optical Depth (VOD) and FLUXNET observed GPP; 4) MTE-GPP (Yao et al., 2018), produced by flux sites observation upscaling approach and Model Tree Ensemble (MTE) algorithm; 5) FLUXCOM GPP (Tramontana et al., 2016), the primary differences between the MTE and FLUXCOM GPP were they used different machine learning algorithms and MTE GPP used more flux sites in southern China; 6) 16 process-based Dynamic Global Vegetation Model (DGVM) simulations (TRENDYv8, Le Quéré et al., 2018).

Given ecosystem GPP was hardly directly measured at a large scale, two additional remote sensed indices were analyzed as well. Solar-Induced Fluorescence (SIF) is found to be strongly correlated with carbon assimilation rate since the leaf-level photosynthesis and fluorescence share the same energy source (Genty et al., 1989). One product is the Contiguous Solar-induced Fluorescence (CSIF), which combined moderate remote sensing reflectance and SIF observations, and enables large-scale SIF estimation with higher temporal and spatial resolutions (Zhang et al., 2018). The other product is Near-Infrared Reflectance of vegetation (NIRv), which is reported as a good proxy of photosynthesis as well (Badgley et al., 2017; Huang et al., 2019).

Environmental information was utilized to analyze driving factors of the dominant drought time scales. Specifically, monthly precipitation and evapotranspiration were derived from Climate Research Unit (CRU TS 4.03, Harris et al., 2020); soil texture data including the percentages of clay, silt and sand was from Resources and Environmental Sciences, Chinese Academy of Sciences. Additionally, in case of mixed information from other disturbances, fire-induced carbon emissions were removed from a monthly Global Fire Emission Database (Randerson et al., 2017).

2.4. *Pre-processing of the datasets*

We addressed the issue of how ecosystem photosynthesis responds to extreme droughts at a growing season scale covering 2000–2015 (the overlapping period of all products). SPEI, GPP, CSIF, NIRv, fire emissions and climate data were firstly interpolated or aggregated into the same spatial resolution of 0.5° × 0.5° using the nearest method. Secondly, those data (P-model, VODCA2GPP, CSIF and NIRv) which are not

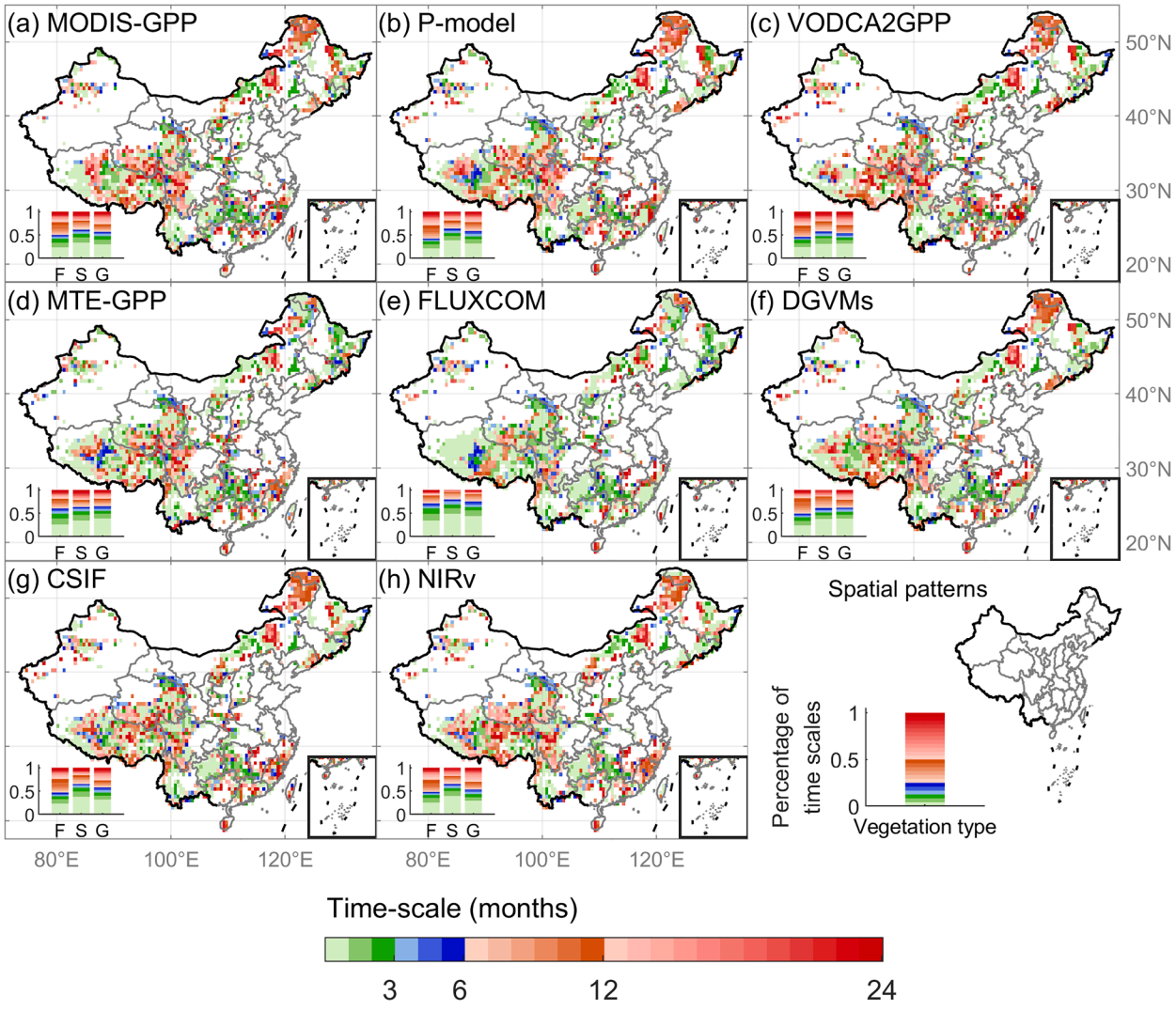

Fig. 5. Spatial patterns of the dominant drought scales of GPP, CSIF, and NIRv. Dominant time scale was the shortest SPEI time scale showing the lowest GPP among 1–24 month time scales with the threshold −1.64 (Eq.(1)). The insets indicate accumulated percentages of dominant time scales for each vegetation type (forest, F; shrubland, S; grassland, G).

monthly were aggregated into monthly temporal resolution by Maximum Value Composite approach (Holben, 1986) to remove noises. Thirdly, the linear trends (the least squares fitting) were removed from the monthly time series. The growing season (GS) ranges were obtained from leaf area index and freeze/thaw data (Zhu et al., 2016), and then GS mean values of SPEI, GPP, CSIF, NIRv, and fire emissions were calculated. To remove the mixed information of other disturbances, potential drought-related GPP was calculated by original GPP adding fire-induced carbon emission.

Anomaly and standardized anomaly of all the data (excluding soil texture) on basis of grids were calculated as Eq.(3) and Eq.(4). In this sense, original values were either centered for inter-comparisons among absolute GPP responses (Fig. 11) or transformed into Z-scores for inter-comparison statistics (Figs. 1-10).

$$A_i = x_i - \mu \tag{3}$$

$$SA_i = \frac{x_i - \mu}{\sigma} \tag{4}$$

where A_i and SA_i are the anomaly and standardized anomaly of one indicator (e.g. GPP or SPEI) in the i^{th} year at one grid, x_i is the growing season mean value in the i^{th} year, μ is the mean and σ is the standard deviation over the study period (2000–2015) at the grid.

3. Results

3.1. GPP responses to combinations of different thresholds and time scales of SPEI

Fig. 3 shows the standardized anomalies of growing season GPP during extreme drought years defined under the thresholds from −1 to −2.5 with a bin of 0.1. There existed discrepancies of GPP responses to extreme droughts when using different thresholds. Generally, more GPP loss was found with stricter thresholds, although a slight increase with the very small threshold (<-1.96) is found among some products (MODIS GPP, VODCA2GPP, MTE-GPP, and FLUXCOM). The threshold is critical for assessing the absolute GPP responses that applying larger thresholds (-1.28, 10% probability for normal distribution) to define droughts shows two thirds of GPP loss comparing with smaller thresholds (-1.96, 2.5%). Further, the differences between GPP responses to short and long-term time scale droughts are not small particularly in GPP estimations from FLUXCOM (Fig. 3e).

Fig. 4 shows the GPP anomalies (s.d.) during extreme drought years under the time scales from 1-month to 48-month. GPP responses varied differently with increasing time scales: the responses presented phenological changes in some products (most optical remote sensing based:

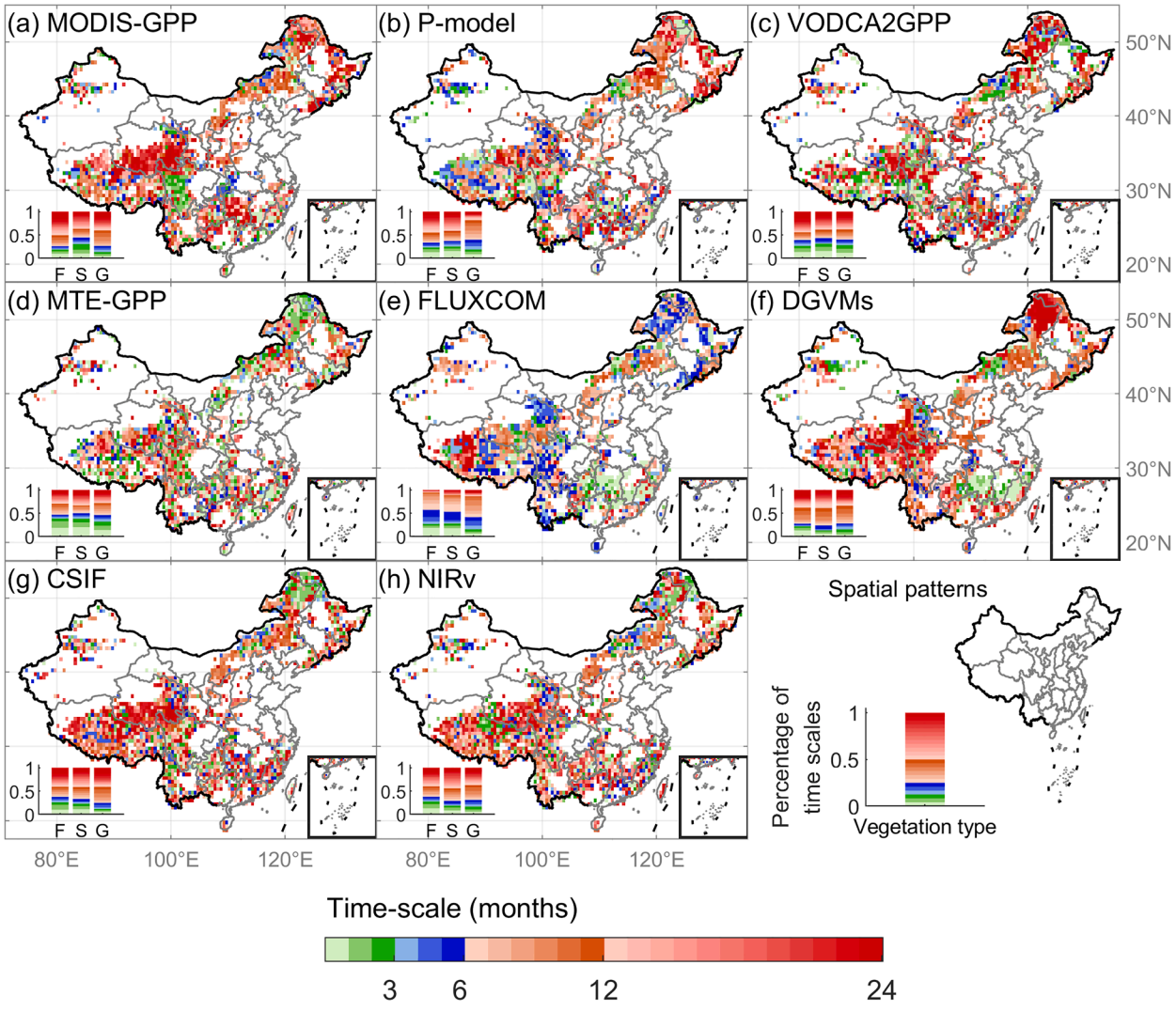

Fig. 6. The same as Fig. 5, but using the correlation method to derive the dominant time scales of SPEI. The dominant time scale was the SPEI time scale showing the largest absolute correlation coefficient with annual GS-GPP among 1–24 month time scales (Eq.(2)).

Fig. 4 a, b, g, and h), while sensitive responses were found during short-term droughts rather than longer-term droughts in other products (Fig. 4 d, e and f, excluding VODCA2GPP, in which GPP responded more sensitively to long-term droughts).

3.2. Spatial patterns of dominant drought time scales

From Figs. 3-4, it is observed that the extents of GPP responses to different time scales of extreme droughts were different, in this sense, the shortest time scale at which droughts caused the most negative GPP response was regarded as the dominant scale (Eq.(3)). Spatial patterns of dominant drought time scales are shown in Fig. 5, and results are relatively consistent among different GPP products (the agreement index Kendall's concordance coefficient W was 0.55). Vegetation in southwest China, arid northern areas, and part of the northeast, tended to respond droughts at shorter time scales (1–6 months); while those vegetated ecosystems in the southeast, Sichuan Province, and part areas in North China and Tibetan Plateau responded to longer-term (greater than12 months) droughts. In terms of different vegetation types, the dominant drought time scales are longer in forests rather than shrubland and grassland (insets in Fig. 5).

Dominant drought time scales derived by the correlation method are shown in Fig. 6, however, the spatial patterns show large discrepancies among different GPP estimations or simulations, and the agreement index was 0.22. Longer dominant time scales were found in the north (a, MODIS GPP; c, VODCA2GPP; f, DGVMs), and there did not show significant differences across biomes. Besides, the correlation coefficients (between GPP and SPEI at the dominant scale) were found to be positive in the northern China (Fig. A.1), and to be negative in southeast China from patterns of most GPP products.

3.3. The dominant time scales and environmental factors

Following previous studies (Vicente-Serrano et al., 2013; Zhang et al., 2017), the relationships between the dominant time scales and water balance were examined (Figs. 7 and 8). Regarding the scales derived by the extreme-based method, vegetation in sub-humid areas tended to respond to droughts at shorter time scales, and the dominant time scales were longer as water balance increased (in humid areas). This phenomenon was also observed among correlation-method derived dominant time scales (Fig. 8) but with a weaker trend (P-model, VODGPP, and NIRv). For those areas of negative water balance, only a few GPP products (P-model, MTE-GPP, DGVMs) show that vegetation in sub-arid areas responded to droughts at longer-term scales (extreme-based) than that in arid areas. In contrast, correlation-based time scales show a strong increasing trend for negative water balance areas (Fig. 8).

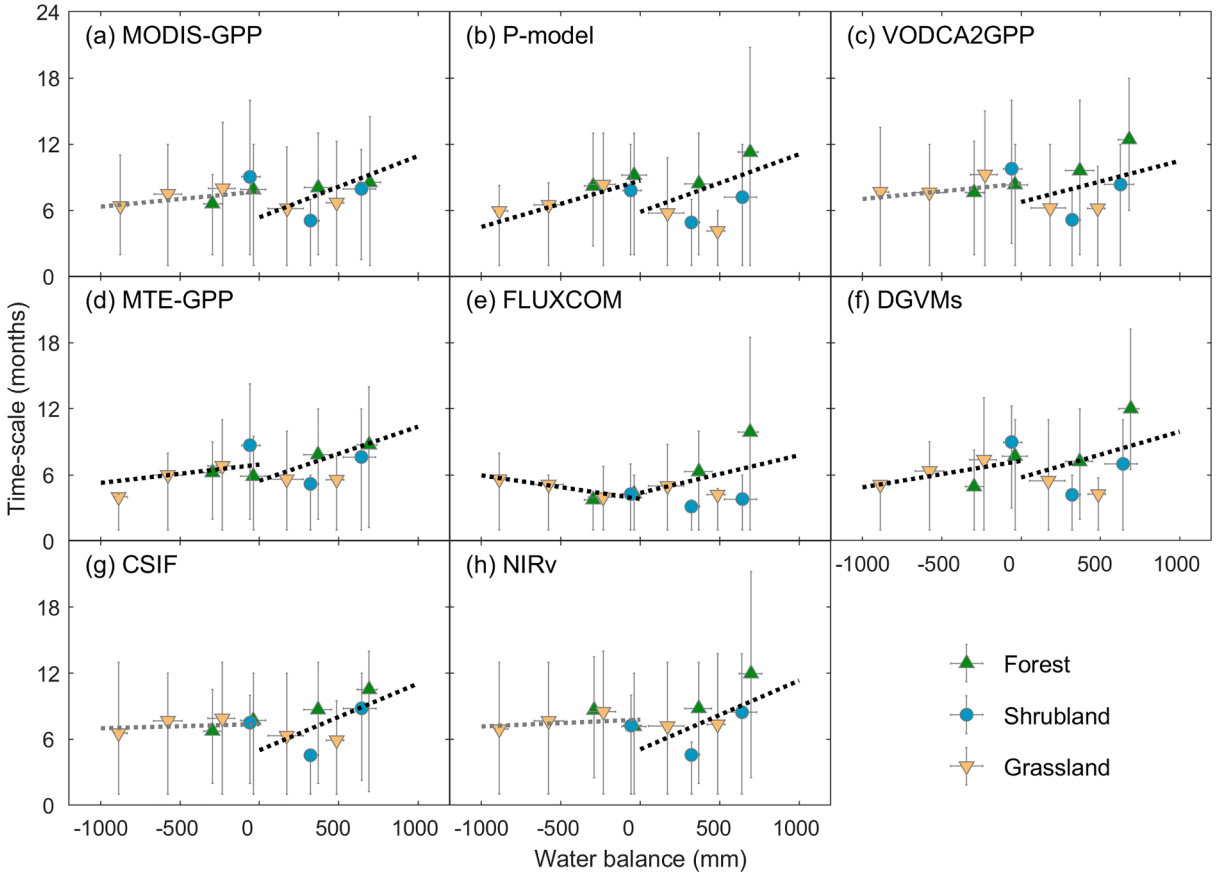

Fig. 7. Relationships between the dominant SPEI time scale and the annual average water balance. The dotted lines indicate linear trends ($p < 0.05$, black; $p \geq 0.05$, grey) of all the gridded data points considering separately negative and positive water balance. The points represent median values and error bars represent the range between the first and the third quantiles of the data.

Additionally, looking into the gradients of water balance, forests responded predominantly to droughts at longer time scales derived by the extreme-based method, which was not captured when applying the correlation-based method.

Soil texture connects with several physiological processes of how a plant absorbs water and nutrients, and is assumed to be potential factors explaining spatial variability of GPP responses to drought time scales. Fig. 9 shows the median dominant time scales located in different soil textures (composition of clay, silt, and sand). Looking into extreme-based derived dominant time scales (Fig. 9a), it is found vegetation planted in loam soil responded to droughts at longer time scales (7–10 months), and those in soils with a larger sand content tended to respond to short-term droughts. Nevertheless, correlation-based derived dominant time scales seem to not differ among soil types with a time scale of 8–11 months.

4. Discussion

4.1. Revisiting GPP responses to different time scales of droughts

SPEI was widely proved to act as a good indicator for regional, continental, and global drought identification (Chen et al., 2013; Li et al., 2019; Schwalm et al., 2017). Meanwhile, the optimal or dominant time scale of SPEI given a specific area has attracted heat discussion, and the correlation approach was employed to address this issue in most previous studies (Gouveia et al., 2017; Vicente-Serrano et al., 2013). That is, SPEI (of the dominant time scale) correlated strongest with vegetation-related index (e.g., NDVI or GPP). However, we demonstrated that drought indicates a climate extreme, and the linear correlation may fail to reveal the real mechanisms for extreme values (Mukaka, 2012). Here we applied both extreme-based and correlation-based method to derive the dominant drought time scale to which GPP respond most sensitively, and highlighted the former be the priority to study extreme drought impacts.

On the one hand, the extreme-based approach was more robust rather than correlation-based method. It can be seen from Fig. 10, the dominant time scales derived among different GPP products are relatively consistent from an extreme point of view. The inter-correlation coefficients can reach 0.66, and the median value is 0.50; while the time scales derived from correlation-based method exhibit large discrepancies with the median inter-correlation coefficient of 0.05. Besides, probably due to similar data sources, higher correlations were found among remote sensing indices (MODIS, P-model, VODGPP, CSIF, and NIRv), and were also found between FLUXCOM and DGVMs.

On the other hand, the time scale is crucial when assessing vegetation responses. Fig. 11 shows the differences between GPP response to the dominant time scale and to one given scale, and 45 ± 26% (six products, mean ± s.d.) of GPP loss will be underestimated if the non-dominant time scale is not selected (Fig. 11). For example, given the study area and period, average P-model GPP response to extreme droughts under dominant time scales was −0.22 gC m^{-2} day^{-1}. Nevertheless, if the time scale was fixed as 6-month (or 12-month), the response was −0.11 (-0.12) gC m^{-2} day^{-1}, which was only half of −0.22. The time scale was also crucial when using the regular method as previous studies (Hua et al., 2017; Vicente-Serrano et al., 2013), and the correlation coefficients between SPEI and vegetation index was increased by ~ 30% if the optimal time scale was selected (Li et al., 2015), although we have demonstrated disadvantages of the

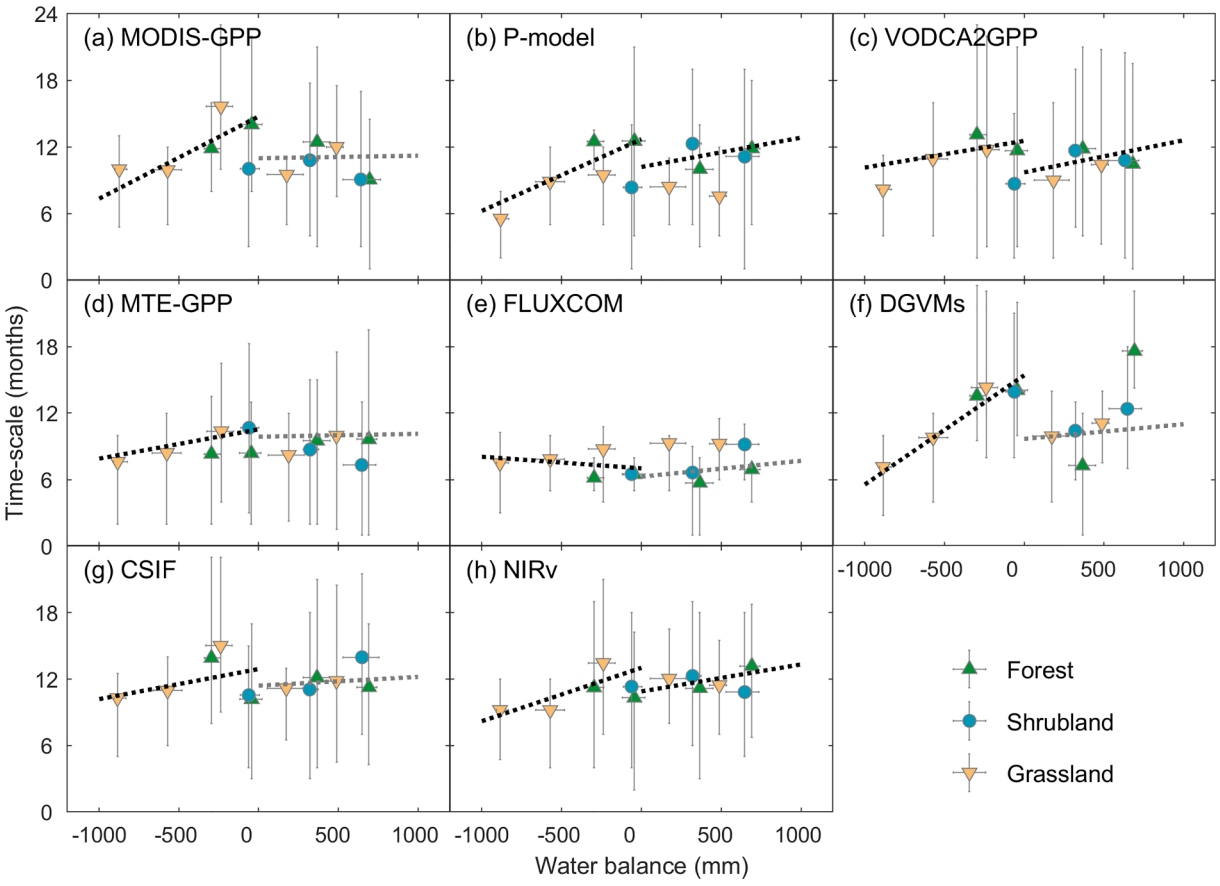

Fig. 8. The same as Fig. 7, but using the correlation method to derive the dominant time scales of SPEI.

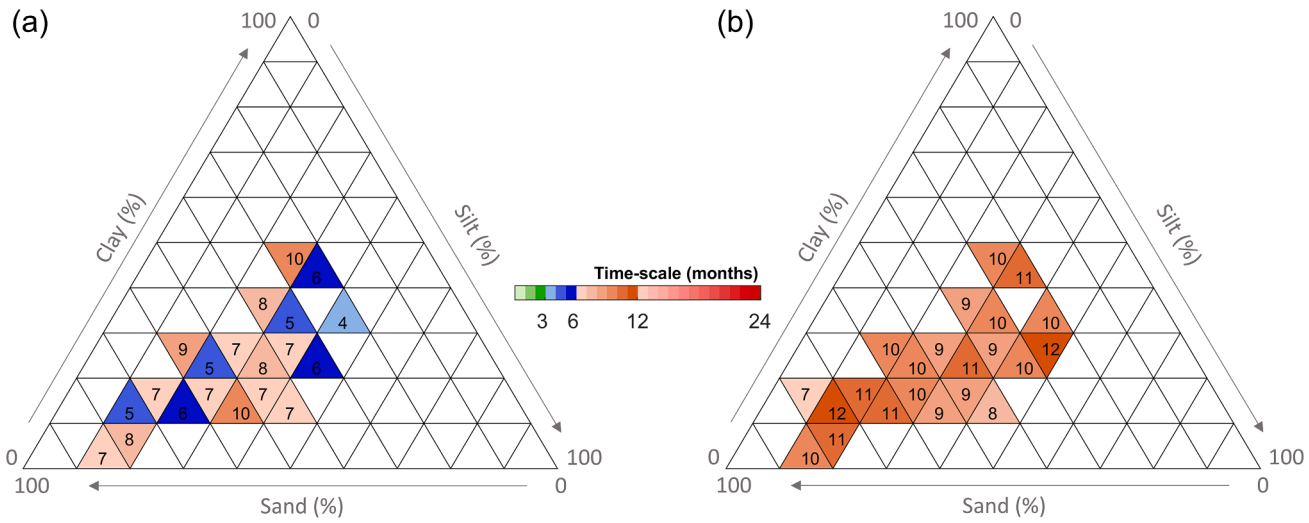

Fig. 9. Median dominant drought time scale (a, extreme-based; b, correlation-based) for different soil textures. The figure is based on the soil textural triangle for soil classification from United States Department of Agriculture (https://www.nrcs.usda.gov/wps/portal/nrcs/detail/soils/survey/tools/?cid=nrcs142p2_054167). And the time scales (number on the small triangles) are the median values among the eight products.

correlation-based method under extreme drought background. In this sense, at which scale that vegetation predominantly responds to extreme droughts should be carefully determined, and we suggest the extreme-based method is an easy and efficient way to address the issue.

4.2. *Dominant time scales and its driving factors*

Looking into the calculation steps of SPEI, the time scale shows how many months' accumulation of water balance (Vicente-Serrano et al., 2010b). The key difference between the two methods (extreme or correlation based) derived time scales, was that how much time is needed to cause the largest losses (even failure) or trigger general vegetation

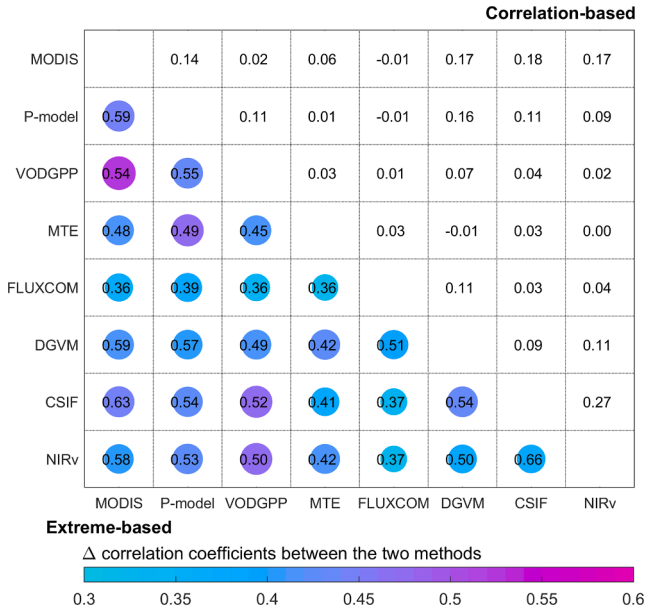

Fig. 10. Inter-correlation coefficients of the dominant drought time scales among different GPP products and GPP-related proxies. The lower triangle shows the results that detected from the extreme-based method, the upper shows the results from the correlation-based method, and the colored circles indicate the difference between the lower and the upper triangle.

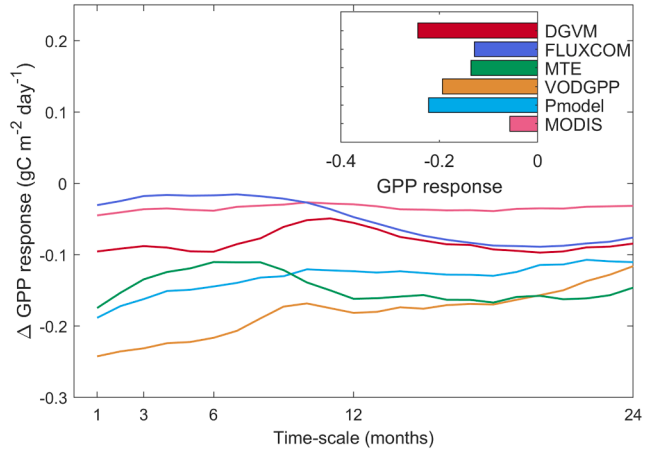

Fig. 11. Differences between GPP response to the dominant time scales and one certain time scale (1–24 months). The inset is the absolute GPP response under the dominant time scale of droughts with the threshold of −1.64.

changes (green or brown). Keep this in mind, several factors could contribute to the spatial heterogeneity of the dominant time scales. Firstly, it is observed that forests responded to extreme droughts at a longer time scale. Forests own deeper rooting systems and can access deeper soil water when water deficit occurs (Li et al., 2019; Xu et al., 2018); such woody vegetation tends to better adopt strategies to keep basic metabolism and to avoid water loss through stomata behaviors (Konings and Gentine, 2017; Lin et al., 2015) and carbon allocation (Trugman et al., 2018). This finding agreed with regional studies in northern China (Xu et al., 2018), northwest pastoral areas (Jiang et al., 2020), and the whole China (Li et al., 2015) based on the correlation approach at monthly scales. Therefore, forests can be more resistant to extreme droughts for a long period rather than grassland.

Secondly, water balance used to play a key role in regulating the response time scales as previous global study (Vicente-Serrano et al., 2013) applying correlations, and they demonstrated arid and humid ecosystems tended to respond to droughts at shorter time scales although with different mechanisms. Correlation-based results in this study were in line with this finding, particularly when water balance was negative, GPP predominantly responded to longer time scale droughts as water balance increased (Fig. 8). However, looking into extreme-based derived scales, humid biomes tended to withstand extreme droughts with a longer time of water deficit (Fig. 7), which was echoing with Zhang et al. (2017). It can be explained by the fact that water balance might not be the controlling factor in humid areas, soil moisture and short-term precipitation might be de-coupled (Wei and Dirmeyer, 2012), and a longer time lag for vegetation growth response to precipitation (Wu et al., 2015) and soil moisture (Chen et al., 2014) existed.

Other environmental factors such as soil texture would contribute to determining at which scale GPP predominantly respond to extreme droughts. Permeability and nutrient content of the soil connect closely to how vegetation copes with drought (Jiang et al., 2020), generally, permeability increases with larger sand proportion (Singh et al., 2020), and nutrients increase with larger clay proportion (Ge et al., 2019). In our study from the extreme point of view, vegetation planted in loam predominantly responded to extreme droughts at longer time scales (7–10 months), since loam well trades off the permeability and nutrient content, and has the better capacity to conserve water and fertility in parallel to Jiang et al. (2020). This phenomenon was not found in correlation-based results, which further implied the uncertainty of deriving dominant scales using linear correlations.

4.3. Uncertainties and limitations

At which time scale ecosystem photosynthesis predominantly responds to extreme droughts was re-studied and we found the extreme-based method be the priority to address this issue. However, there remained some uncertainties to be carefully considered. On the one hand, although considerable consistency was observed among time scales derived from six state-of-the-art GPP estimations and two additional proxies CSIF and NIRv (He et al., 2021), uncertainties existed from data sources. Each product has its disadvantages in displaying large-scale GPP, for example, flux sites upscaling GPP may underestimate the inter-annual variability (Jung et al., 2020) and the response time since GPP was trained by concurrent climate data. Besides, simplified DGVMs may not fully represent the complex ecological processes (Wang et al., 2020), and correlations between SIF and GPP are not stable and covary with climatic factors (Chen et al., 2021). On the other hand, drought characteristics such as legacy (Anderegg et al., 2015) and flash drought (Pendergrass et al., 2020) were not considered in our study, which might lead to uncertainties and should be further examined.

5. Conclusion

Aiming at explore the dominant drought time scales, in this paper, we revisited the responses of ecosystem photosynthesis to extreme droughts with six state-of-the-art GPP estimations, CSIF and NIRv, based on which these conclusions can be drawn:

(1) Responses of GPP varied when using different thresholds and time scales of SPEI to define extreme droughts, generally, more GPP loss was found with more strict thresholds, relationships between GPP response and SPEI time scales (1–48 months) were nonlinear, and thus a dominant time scale of SPEI existed.
(2) The extreme-based method is more reasonable and robust for deriving the dominant time scales. The spatial patterns among different products were relatively consistent rather than that derived from correlations. If the dominant time scale was not selected, the GPP responses to extreme droughts might be underestimated by 45 ± 26%.

(3) Factors driving the spatial heterogeneity of dominant time scales included vegetation type, water balance, and soil textures. In general, forests responded to extreme droughts at a longer time scale than shallow-rooted grassland and cropland. GPP in humid biomes can be more resistant to long-term droughts, which was not in line with findings from correlations, implying the correlation approach may fail to reflect and focus on the extreme negative situation. The dominant time scales for vegetation planted in loam were longer since loam has a better capacity to conserve water and fertility.

Our study highlighted it should be careful when selecting the dominant drought time scale, and the extreme-based method was recommended. In further studies, it is suggested to consider the effects of drought legacy and flash droughts on the response of photosynthesis to drought time scales.

Declaration of Competing Interest

The authors declare that they have no known competing financial interests or personal relationships that could have appeared to influence the work reported in this paper.

Acknowledgement

This study was supported by the Key Program of Frontier Sciences of the Chinese Academy of Sciences (QYZDY-SSW-SMCO11-2) and National Field Station for Forest Ecosystem in Shennongjia (60216F1001; E0217G2001). We thank TRENDY modeling group for providing DGVM simulation data.

Appendix A. Supplementary data

Supplementary data to this article can be found online at https://doi.org/10.1016/j.ecolind.2022.108630.

References

Al-Yaari, A., Wigneron, J.-P., Ciais, P., Reichstein, M., Ballantyne, A., Ogée, J., Ducharne, A., Swenson, J.J., Frappart, F., Fan, L., Wingate, L., Li, X., Hufkens, K., Knapp, A.K., 2020. Asymmetric responses of ecosystem productivity to rainfall anomalies vary inversely with mean annual rainfall over the conterminous United States. Glob. Chang. Biol. 26 (12), 6959–6973.

Allen, C.D., Macalady, A.K., Chenchouni, H., Bachelet, D., McDowell, N., Vennetier, M., Kitzberger, T., Rigling, A., Breshears, D.D., Hogg, E.H., Gonzalez, P., Fensham, R., Zhang, Z., Castro, J., Demidova, N., Lim, J.-H., Allard, G., Running, S.W., Semerci, A., Cobb, N., 2010. A global overview of drought and heat-induced tree mortality reveals emerging climate change risks for forests. Forest. Ecol. Manag. 259 (4), 660–684.

Anav, A., Friedlingstein, P., Beer, C., Ciais, P., Harper, A., Jones, C., Murray-Tortarolo, G., Papale, D., Parazoo, N.C., Peylin, P., Piao, S., Sitch, S., Viovy, N., Wiltshire, A., Zhao, M., 2015. Spatiotemporal patterns of terrestrial gross primary production: A review. Rev. Geophys. 53 (3), 785–818.

Anderegg, W.R.L., Schwalm, C., Biondi, F., et al., 2015. Pervasive drought legacies in forest ecosystems and their implications for carbon cycle models. Science 349 (6247), 528–532.

Anderegg, W.R.L., Trugman, A.T., Badgley, G., Konings, A.G., Shaw, J., 2020. Divergent forest sensitivity to repeated extreme droughts. Nat. Clim. Chang. 10 (12), 1091–1095.

Badgley, G., Field, C.B., Berry, J.A., 2017. Canopy near-infrared reflectance and terrestrial photosynthesis. Sci. Adv. 3 (3), e1602244.

Chen, A., Mao, J., Ricciuto, D., Lu, D., Xiao, J., Li, X., Thornton, P.E., Knapp, A.K., 2021. Seasonal changes in GPP/SIF ratios and their climatic determinants across the Northern Hemisphere. Glob. Chang. Biol. 27 (20), 5186–5197.

Chen, T., de Jeu, R.A.M., Liu, Y.Y., van der Werf, G.R., Dolman, A.J., 2014. Using satellite based soil moisture to quantify the water driven variability in NDVI: A case study over mainland Australia. Remote Sens. Environ. 140, 330–338.

Chen, T., Werf, G.R., Jeu, R.A.M., Wang, G., Dolman, A.J., 2013. A global analysis of the impact of drought on net primary productivity. Hydrol. Earth. Syst. Sci. 17 (10), 3885–3894.

Deng, Y., Wang, X., Wang, K., Ciais, P., Tang, S., Jin, L., Li, L., Piao, S., 2021. Responses of vegetation greenness and carbon cycle to extreme droughts in China. Agr. Forest. Meteorol. 298-299, 108307. https://doi.org/10.1016/j.agrformet.2020.108307.

Doughty, C.E., Metcalfe, D.B., Girardin, C.A.J., et al., 2015. Drought impact on forest carbon dynamics and fluxes in Amazonia. Nature 519 (7541), 78–82.

Editorial Board of Vegetation Map of China, 2007. Chinese Academy of Sciences. Vegetation Map of the People's Republic of China (1:1000000) (Digital Version). Geology Press, Beijing, China.

Ge, N., Wei, X., Wang, X., Liu, X., Shao, M., Jia, X., Li, X., Zhang, Q., 2019. Soil texture determines the distribution of aggregate-associated carbon, nitrogen and phosphorous under two contrasting land use types in the Loess Plateau. Catena 172, 148–157.

Genty, B., Briantais, J.-M., Baker, N.R., 1989. The relationship between the quantum yield of photosynthetic electron transport and quenching of chlorophyll fluorescence. Biochim. Biophys. Acta (BBA) – Gen. Sub. 990 (1), 87–92.

Gouveia, C.M., Trigo, R.M., Beguería, S., Vicente-Serrano, S.M., 2017. Drought impacts on vegetation activity in the Mediterranean region: An assessment using remote sensing data and multi-scale drought indicators. Glob. Planet Change 151, 15–27.

Harris, I., Osborn, T.J., Jones, P., Lister, D., 2020. Version 4 of the CRU TS monthly high-resolution gridded multivariate climate dataset. Sci. Data 7 (109). https://doi.org/10.1038/s41597-020-0453-3.

He, B., Chen, C., Lin, S., Yuan, W., Chen, H.W., Chen, D., Zhang, Y., Guo, L., Zhao, X., Liu, X., Piao, S., Zhong, Z., Wang, R., Tang, R., 2021. Worldwide impacts of atmospheric vapor pressure deficit on the interannual variability of terrestrial carbon sinks. Natl. Sci. Rev. https://doi.org/10.1093/nsr/nwab150.

Holben, B.N., 1986. Characteristics of maximum-value composite images from temporal avhrr data. Int. J. Remote. Sens. 7 (11), 1417–1434.

Hua, T., Wang, X., Zhang, C., Lang, L., Li, H., 2017. Responses of vegetation activity to drought in Northern China. Land. Degrad. Dev. 28 (7), 1913–1921.

Huang, K., Yi, C., Wu, D., Zhou, T., Zhao, X., Blanford, W.J., Wei, S., Wu, H., Ling, D.u., Li, Z., 2015. Tipping point of a conifer forest ecosystem under severe drought. Environ. Res. Lett. 10 (2), 024011. https://doi.org/10.1088/1748-9326/10/2/024011.

Huang, M., Piao, S., Ciais, P., Peñuelas, J., Wang, X., Keenan, T.F., Peng, S., Berry, J.A., Wang, K., Mao, J., Alkama, R., Cescatti, A., Cuntz, M., De Deurwaerder, H., Gao, M., He, Y., Liu, Y., Luo, Y., Myneni, R.B., Niu, S., Shi, X., Yuan, W., Verbeeck, H., Wang, T., Wu, J., Janssens, I.A., 2019. Air temperature optima of vegetation productivity across global biomes. Nat. Ecol. Evol. 3 (5), 772–779.

IPCC, 2014. Climate Change 2014: Synthesis Report. Contribution of Working Groups I, II and III to the Fifth Assessment Report of the Intergovernmental Panel on Climate Change, Geneva, Switzerland.

Jiang, P., Ding, W., Yuan, Y.e., Ye, W., 2020. Diverse response of vegetation growth to multi-time-scale drought under different soil textures in China's pastoral areas. J. Environ. Manage. 274, 110992. https://doi.org/10.1016/j.jenvman.2020.110992.

Jung, M., Schwalm, C., Migliavacca, M., et al., 2020. Scaling carbon fluxes from eddy covariance sites to globe: synthesis and evaluation of the FLUXCOM approach. Biogeosciences 17 (5), 1343–1365.

Knapp, A.K., Ciais, P., Smith, M.D., 2017. Reconciling inconsistencies in precipitation-productivity relationships: implications for climate change. New Phytol. 214 (1), 41–47.

Konings, A.G., Gentine, P., 2017. Global variations in ecosystem-scale isohydricity. Glob. Chang. Biol. 23 (2), 891–905.

Le Quéré, C., Andrew, R.M., Friedlingstein, P., et al., 2018. Global carbon budget 2018. Earth Syst. Sci. Data 10 (4), 2141–2194.

Li, C., Leal Filho, W., Yin, J., Hu, R., Wang, J., Yang, C., Yin, S., Bao, Y., Ayal, D.Y., 2018. Assessing vegetation response to multi-time-scale drought across inner Mongolia plateau. J. Clean. Prod. 179, 210–216.

Li, X., Li, Y., Chen, A., Gao, M., Slette, I.J., Piao, S., 2019. The impact of the 2009/2010 drought on vegetation growth and terrestrial carbon balance in Southwest China. Agr. Forest. Meteorol. 269-270, 239–248.

Li, Z., Zhou, T., Zhao, X., Huang, K., Gao, S., Wu, H., Luo, H., 2015. Assessments of drought impacts on vegetation in china with the optimal time scales of the climatic drought index. Int. J. Environ. Res. Public Health 12 (7), 7615–7634.

Lin, Y.-S., Medlyn, B.E., Duursma, R.A., et al., 2015. Optimal stomatal behaviour around the world. Nat. Clim. Chang. 5 (5), 459–464.

Maurya, S.P., Singh, P.K., Ohri, A., Singh, R., 2020. Identification of indicators for sustainable urban water development planning. Ecol. Indic. 108, 105691. https://doi.org/10.1016/j.ecolind.2019.105691.

Mishra, A.K., Singh, V.P., 2010. A review of drought concepts. J. Hydrol. 391 (1-2), 202–216.

Mukaka, M.M., 2012. Statistics corner: A guide to appropriate use of correlation coefficient in medical research. Malawi Med. J. 24 (3), 69–71.

Pendergrass, A.G., Meehl, G.A., Pulwarty, R., et al., 2020. Flash droughts present a new challenge for subseasonal-to-seasonal prediction. Nat. Clim. Chang. 10 (3), 191–199.

Piao, S., Wang, X., Wang, K., Li, X., Bastos, A., Canadell, J.G., Ciais, P., Friedlingstein, P., Sitch, S., 2020. Interannual variation of terrestrial carbon cycle: Issues and perspectives. Glob. Chang. Biol. 26 (1), 300–318.

Randerson, J.T., Van Der Werf, G.R., Giglio, L., Collatz, G.J. and Kasibhatla, P.S., 2017. Global Fire Emissions Database, Version 4.1 (GFEDv4). ORNL Distributed Active Archive Center.

Reichstein, M., Bahn, M., Ciais, P., et al., 2013. Climate extremes and the carbon cycle. Nature 500 (7462), 287–295.

Schwalm, C.R., Anderegg, W.R.L., Michalak, A.M., et al., 2017. Global patterns of drought recovery. Nature 548 (7666), 202–205.

Singh, V.K., Kumar, D., Kashyap, P.S., Singh, P.K., Kumar, A., Singh, S.K., 2020. Modelling of soil permeability using different data driven algorithms based on physical properties of soil. J. Hydrol. 580, 124223. https://doi.org/10.1016/j.jhydrol.2019.124223.

Sitch, S., Huntingford, C., Gedney, N., Levy, P.E., Lomas, M., Piao, S.L., Betts, R., Ciais, P., Cox, P., Friedlingstein, P., Jones, C.D., Prentice, I.C., Woodward, F.I., 2008. Evaluation of the terrestrial carbon cycle, future plant geography and climate-carbon cycle feedbacks using five Dynamic Global Vegetation Models (DGVMs). Glob. Chang. Biol. 14 (9), 2015–2039.

Slette, I.J., Post, A.K., Awad, M., Even, T., Punzalan, A., Williams, S., Smith, M.D., Knapp, A.K., 2019. How ecologists define drought, and why we should do better. Glob. Chang. Biol. 25 (10), 3193–3200.

Slette, I.J., Smith, M.D., Knapp, A.K., Vicente-Serrano, S.M., Camarero, J.J., Beguería, S., 2020. Standardized metrics are key for assessing drought severity. Glob. Chang. Biol. 26 (2) https://doi.org/10.1111/gcb.v26.210.1111/gcb.14899.

Stocker, B.D., Zscheischler, J., Keenan, T.F., Prentice, I.C., Peñuelas, J., Seneviratne, S.I., 2018. Quantifying soil moisture impacts on light use efficiency across biomes. New Phytol. 218 (4), 1430–1449.

Stocker, B.D., Zscheischler, J., Keenan, T.F., Prentice, I.C., Seneviratne, S.I., Peñuelas, J., 2019. Drought impacts on terrestrial primary production underestimated by satellite monitoring. Nat. Geosci. 12 (4), 264–270.

Su, B., Huang, J., Fischer, T., et al., 2018. Drought losses in China might double between the 1.5 degrees C and 2.0 degrees C warming. Proc. Natl. Acad. Sci. U.S.A. 115 (42), 10600–10605.

Tramontana, G., Jung, M., Schwalm, C.R., Ichii, K., Camps-Valls, G., Ráduly, B., Reichstein, M., Arain, M.A., Cescatti, A., Kiely, G., Merbold, L., Serrano-Ortiz, P., Sickert, S., Wolf, S., Papale, D., 2016. Predicting carbon dioxide and energy fluxes across global FLUXNET sites with regression algorithms. Biogeosciences 13 (14), 4291–4313.

Trugman, A.T., Detto, M., Bartlett, M.K., Medvigy, D., Anderegg, W.R.L., Schwalm, C., Schaffer, B., Pacala, S.W., Cameron, D., 2018. Tree carbon allocation explains forest drought-kill and recovery patterns. Ecol. Lett. 21 (10), 1552–1560.

van der Laan-Luijkx, I.T., van der Velde, I.R., Krol, M.C., Gatti, L.V., Domingues, L.G., Correia, C.S.C., Miller, J.B., Gloor, M., van Leeuwen, T.T., Kaiser, J.W., Wiedinmyer, C., Basu, S., Clerbaux, C., Peters, W., 2015. Response of the Amazon carbon balance to the 2010 drought derived with CarbonTracker South America. Global Biogeochem. Cy. 29 (7), 1092–1108.

Vicente-Serrano, S.M., Beguería, S., López-Moreno, J.I., 2010a. A multiscalar drought index sensitive to global warming: the standardized precipitation evapotranspiration index. J. Clim. 23 (7), 1696–1718.

Vicente-Serrano, S.M., Beguería, S., López-Moreno, J.I., Angulo, M. and El Kenawy, A., 2010b. A New Global 0.5° Gridded Dataset (1901–2006) of a Multiscalar Drought Index: Comparison with Current Drought Index Datasets Based on the Palmer Drought Severity Index. J. Hydrometeorol. 11(4), 1033–1043.

Vicente-Serrano, S.M., Gouveia, C., Camarero, J.J., et al., 2013. Response of vegetation to drought time-scales across global land biomes. Proc. Natl. Acad. Sci. USA 110 (1), 52–57.

Wang, K., Wang, Y., Wang, X., et al., 2020. Causes of slowing-down seasonal CO2 amplitude at Mauna Loa. Glob. Chang. Biol. 26 (8), 4462–4477.

Wei, J., Dirmeyer, P.A., 2012. Dissecting soil moisture-precipitation coupling. Geophys. Res. Lett. 39 (19), n/a–n/a.

Wild, B., Teubner, I., Moesinger, L., et al., 2021. VODCA2GPP - A new global, long-term (1988–2020) GPP dataset from microwave remote sensing. Earth Syst. Sci. Data Discuss. 2021, 1–37.

Wolf, S., Keenan, T.F., Fisher, J.B., Baldocchi, D.D., Desai, A.R., Richardson, A.D., Scott, R.L., Law, B.E., Litvak, M.E., Brunsell, N.A., Peters, W., van der Laan-Luijkx, I. T., 2016. Warm spring reduced carbon cycle impact of the 2012 US summer drought. Proc. Natl. Acad. Sci. U.S.A. 113 (21), 5880–5885.

World Meteorological Organization and Global Water Partnership, 2016. Handbook of Drought Indicators and Indices, Integrated Drought Management Programme (IDMP), Geneva.

Wu, D., Vargas G, G., Powers, J.S. et al., 2021. Reduced ecosystem resilience quantifies fine-scale heterogeneity in tropical forest mortality responses to drought. Glob. Chang. Biol. n/a(n/a).

Wu, D., Zhao, X., Liang, S., Zhou, T., Huang, K., Tang, B., Zhao, W., 2015. Time-lag Effects of Global Vegetation Responses to Climate Change. Glob. Chang. Biol. 21 (9), 3520–3531.

Wu, J., Liu, Z., Yao, H., Chen, X., Chen, X., Zheng, Y., He, Y., 2018. Impacts of reservoir operations on multi-scale correlations between hydrological drought and meteorological drought. J. Hydrol. 563, 726–736.

Xie, X., Li, A., Tan, J., Lei, G., Jin, H., Zhang, Z., 2020. Uncertainty analysis of multiple global GPP datasets in characterizing the lagged effect of drought on photosynthesis. Ecol. Indic. 113, 106224. https://doi.org/10.1016/j.ecolind.2020.106224.

Xu, C., McDowell, N.G., Fisher, R.A., Wei, L., Sevanto, S., Christoffersen, B.O., Weng, E., Middleton, R.S., 2019. Increasing impacts of extreme droughts on vegetation productivity under climate change. Nat. Clim. Chang. 9 (12), 948–953.

Xu, H.-J., Wang, X.-P., Zhao, C.-Y., Yang, X.-M., 2018. Diverse responses of vegetation growth to meteorological drought across climate zones and land biomes in northern China from 1981 to 2014. Agr. Forest. Meteorol. 262, 1–13.

Xu, X., Piao, S., Wang, X., Chen, A., Ciais, P., Myneni, R.B., 2012. Spatio-temporal patterns of the area experiencing negative vegetation growth anomalies in China over the last three decades. Environ. Res. Lett. 7 (3), 035701. https://doi.org/10.1088/1748-9326/7/3/035701.

Yao, Y., Wang, X., Li, Y., et al., 2018. Spatiotemporal pattern of gross primary productivity and its covariation with climate in China over the last thirty years. Glob. Chang. Biol. 24 (1), 184–196.

Yuan, W., Cai, W., Chen, Y., et al., 2016. Severe summer heatwave and drought strongly reduced carbon uptake in Southern China. Sci. Rep. 6 (1) https://doi.org/10.1038/srep18813.

Zhang, Q., Kong, D., Singh, V.P., Shi, P., 2017. Response of vegetation to different time-scales drought across China: Spatiotemporal patterns, causes and implications. Glob. Planet Change 152, 1–11.

Zhang, Y., Joiner, J., Alemohammad, S.H., Zhou, S., Gentine, P., 2018. A global spatially contiguous solar-induced fluorescence (CSIF) dataset using neural networks. Biogeosciences 15 (19), 5779–5800.

Zhang, Y., Xiao, X., Zhou, S., Ciais, P., McCarthy, H., Luo, Y., 2016. Canopy and physiological controls of GPP during drought and heat wave. Geophys. Res. Lett. 43 (7), 3325–3333.

Zhao, M., Heinsch, F.A., Nemani, R.R., Running, S.W., 2005. Improvements of the MODIS terrestrial gross and net primary production global data set. Remote Sens. Environ. 95 (2), 164–176.

Zhao, M., Running, S.W., 2010. Drought-induced reduction in global terrestrial net primary production from 2000 through 2009. Science 329 (5994), 940–943.

Zhao, X., Wei, H., Liang, S., Zhou, T., He, B., Tang, B., Wu, D., 2015. Responses of Natural Vegetation to Different Stages of Extreme Drought during 2009–2010 in Southwestern China. Remote Sens. 7 (10), 14039–14054.

Zhu, Z., Piao, S., Myneni, R.B., et al., 2016. Greening of the Earth and its drivers. Nat. Clim. Chang. 6 (8), 791–795.

Zscheischler, J., Mahecha, M.D., von Buttlar, J., et al., 2014. A few extreme events dominate global interannual variability in gross primary production. Environ. Res. Lett. 9 (3), 035001. https://doi.org/10.1088/1748-9326/9/3/035001.